

## APPENDIX A

### RELAXATION OSCILLATORS

#### A1 Introduction

Relaxation oscillators are a generic type of oscillators. They are continuous but highly nonlinear and are typically thought to represent a class of oscillators different from the familiar harmonic, or sinusoidal oscillators. A reader unfamiliar with concepts such as nullclines, limit cycles, sinusoidal oscillators, and relaxation oscillators may find this Appendix useful. We also graphically describe the transition from sinusoidal to relaxation type oscillations. In Section A2 we describe four types of trajectories that arise in a pair of coupled oscillators.

The relaxation oscillators we examine are the Terman-Wang oscillators [Terman and Wang, 1995] that are based on the Morris-Lecar model of neural behavior [Morris and Lecar, 1981]. The relaxation oscillator used here is the same as that used in Chapter 3. All but one of the parameters have been fixed for simplicity,

$$\frac{dx}{dt} = \dot{x} = 3x - x^3 - y \tag{A.1.a}$$

$$\frac{dy}{dt} = \dot{y} = \epsilon (3 + 42 \tanh(10x) - y) \tag{A.1.b}$$

This is a pair of coupled first order nonlinear differential equations. A starting point for understanding this system is to examine its nullclines, which are shown in Figure 64. The cubic shaped curve represents the x-nullcline, or the curve along which  $\dot{x} = 0$ . This is given by  $\dot{x} = 3x - x^3 - y = 0$ , or  $y = 3x - x^3$ . We will frequently refer to the cubic as consisting of three different “branches”; the middle branch, which passes through the point (0,0) and connects the two local extrema, and the left and right branches, which extend from the local extrema to  $+\infty$  and  $-\infty$  respectively. The y-nullcline,  $\dot{y} = 0$ , is given by  $y = 3 + 42 \tanh(10x)$ . This hyperbolic tangent results in a sigmoid shaped curve, but because the argument of the hyperbolic tangent is multiplied by 10, the function looks more like a step function. The nullclines divide the x-y plane into four portions.

Above the  $x$ -nullcline, the  $x$ -velocity is negative, thus all values of  $x$  in that region of the plane will result in a negative  $x$ -velocity (as indicated by the arrows in Figure 64). Below the  $x$ -nullcline, the  $x$ -velocity is positive, thus motion is in the positive  $x$ -direction. Analogous statements can be made for the  $y$ -nullcline. From these qualitative directions of motion one can see how a periodic trajectory might arise. However, there are several further requirements needed for oscillatory behavior to exist and one can find the details in [Minorsky, 1962].

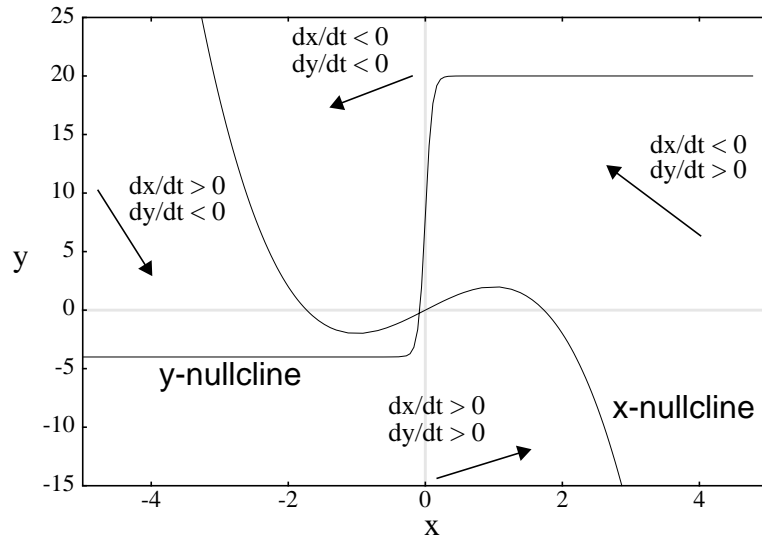


Figure 64. A diagram showing the qualitative direction of motion for system (A.1). The two curves represent the  $x$ - and  $y$ -nullclines.

The parameter  $\epsilon$  describes the two different time scales that define relaxation oscillators. If  $\epsilon$  is of  $O(1)$ , then the oscillator is said to be in the sinusoidal regime because it can have a nearly uniform speed of motion along its limit cycle. For small  $\epsilon$ , the oscillator begins to exhibit two distinct time scales, or it has two different speeds of motion along disparate portions of its limit cycle. As one varies  $\epsilon$ , the equations change smoothly from sinusoidal oscillators to relaxation oscillators. Figure 65A displays the limit cycle for  $\epsilon = 1$  for (A.1) and one can see that it does appear qualitatively sinusoidal, as do the temporal evolution of both variables in Figure 65B. In Figure 66A, B, and C we display limit cycles and temporal evolution of the variables for progressively smaller values of  $\epsilon$  ( $\epsilon = 0.33$ ,  $\epsilon = 0.1$ ,  $\epsilon = 0.01$ ). As  $\epsilon$  becomes smaller, the velocity in the  $y$ -direction becomes smaller, and comparatively, motion in the  $x$ -direction becomes faster. In Figure 66C,  $\epsilon = 0.01$  and motion from the left branch to the right branch (and vice-versa) occurs quickly. Motion along the cubic (in the  $y$ -direction) is dominated by the slow parameter and occurs approximately 100 times slower than motion between the branches.

The term relaxation oscillator was first coined by van der Pol in 1926 [van der Pol, 1926]. The transition from a sinusoidal oscillator (as one might classify the limit cycle shown in Figure 65) to a relaxation oscillator (the limit cycle in Figure 66C) is

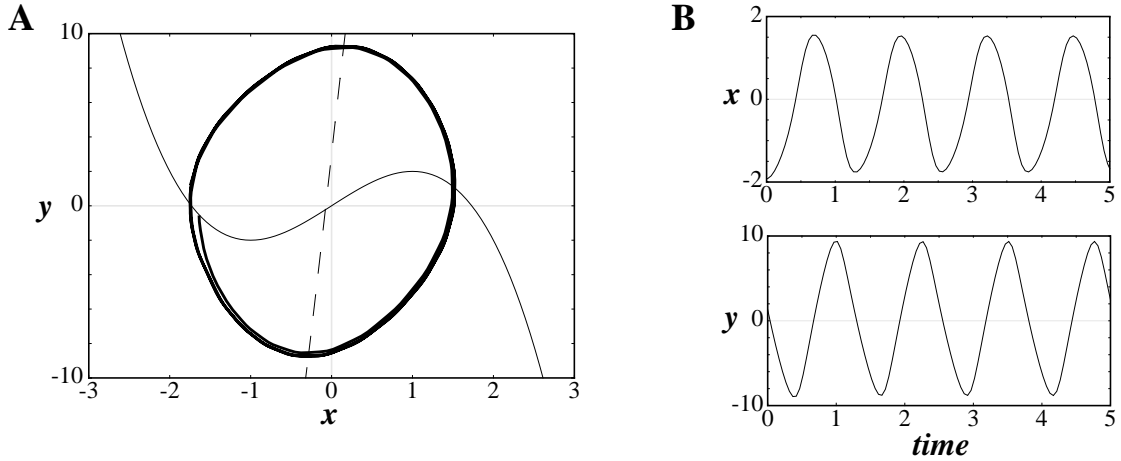


Figure 65. (A) The limit (thick curve) cycle for (A.1) with  $\varepsilon = 1.0$ . The x- and y-nullclines are the thinner curves. (B) The temporal evolution of the x-variable and the y-variable.

smooth, and not clearly defined to our knowledge, but the distinction is an important qualitative one. Study still continues in understanding the differences between sinusoidal and relaxation oscillators.

When  $\varepsilon = 0$  an oscillator is said to be in the singular limit and the relative speed of motion in the x-direction is infinitely fast in comparison with the speed of motion along the outer branches. The transition between the left and right branches thus occurs instantaneously, with no change in the y-variable. In the singular limit, and if the form of (A.1) is sufficiently simple, the speed of motion can be found analytically for y-variable and the speed of motion for the x-variable can be ignored, since it is instantaneous during the jumps. For small values of  $\varepsilon$ , a perturbation analysis can be performed [Bender and Orszag, 1978].

## A2 A Pair of Relaxation Oscillators

A pair of coupled relaxation oscillators is defined as follows,

$$\dot{x}_1 = 3x_1 - x_1^3 - y_1 + \alpha_R S(x_2) \quad (\text{A.2.a})$$

$$\dot{y}_1 = \varepsilon (\lambda + \gamma \tanh(\beta x_1) - y_1) \quad (\text{A.2.b})$$

$$\dot{x}_2 = 3x_2 - x_2^3 - y_2 + \alpha_R S(x_1) \quad (\text{A.2.c})$$

$$\dot{y}_2 = \varepsilon (\lambda + \gamma \tanh(\beta x_2) - y_2) \quad (\text{A.2.d})$$

$$S(x) = [1 + \exp(\kappa(\theta - x))]^{-1} \quad (\text{A.2.e})$$

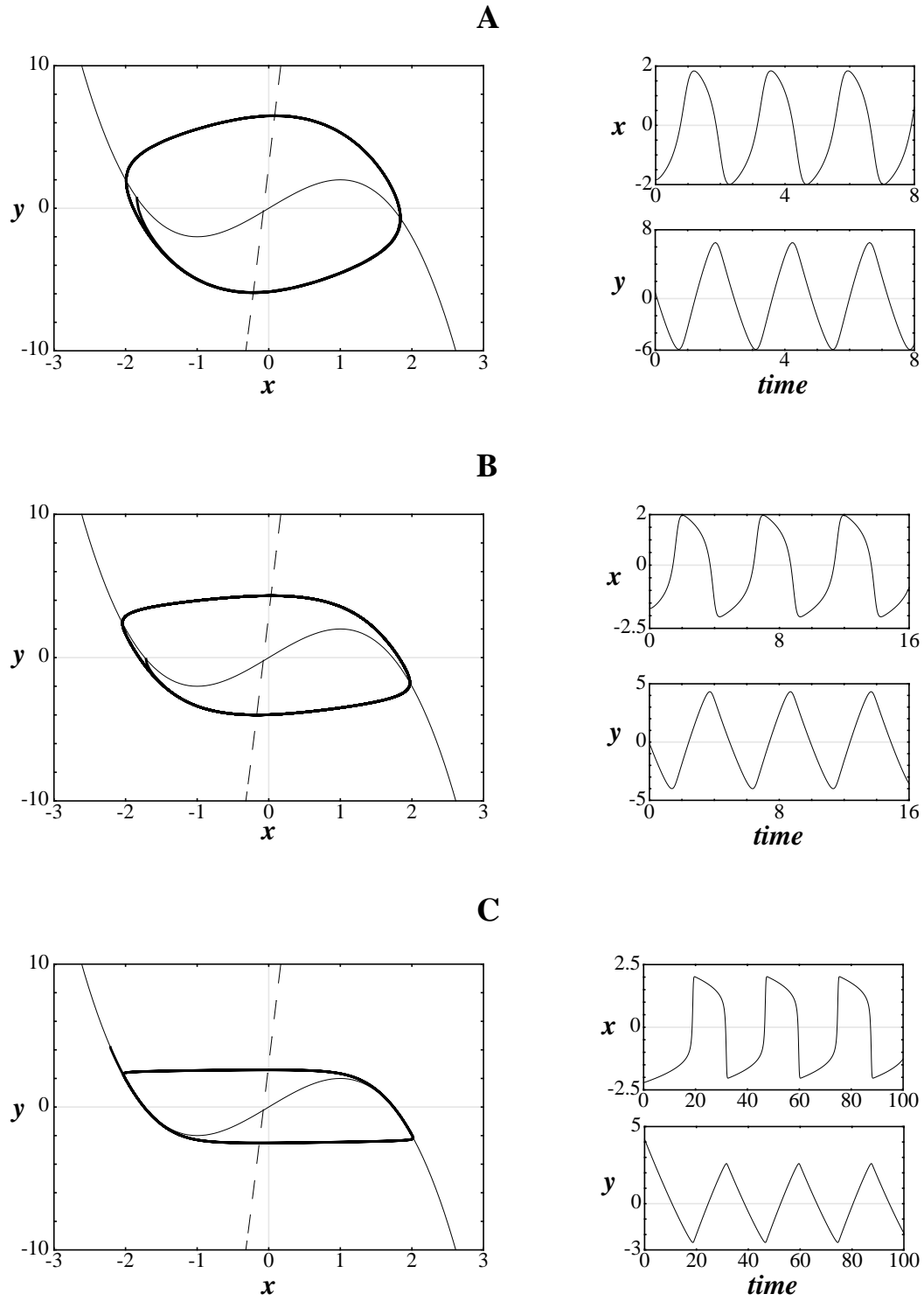


Figure 66. Three different limit cycles and their respective plots as a function of time are shown for three different values of  $\epsilon$ . (A)  $\epsilon = 0.33$ . (B)  $\epsilon = 0.1$ . (C)  $\epsilon = 0.01$ .

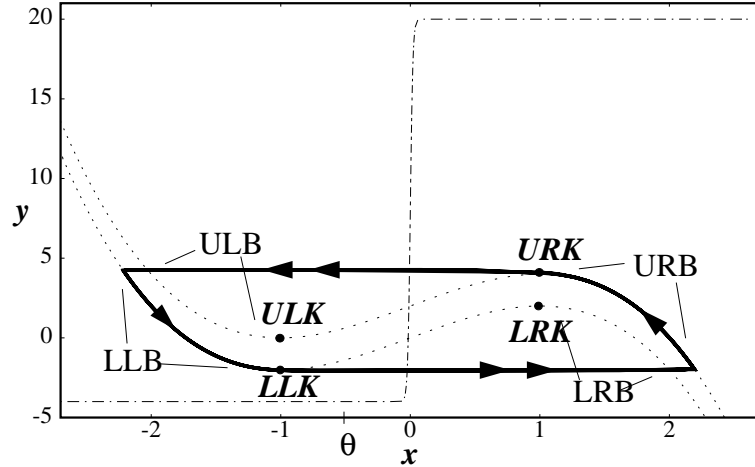


Figure 67. A plot of the nullclines and the synchronous limit cycle of a relaxation oscillator defined in (A.2). The dotted cubics are the excited and unexcited  $x$ -nullclines, and the dash-dot curve is the  $y$ -nullcline. The thick solid curve represents the synchronous limit cycle for a pair of oscillators, which is the result of numerical calculation. The parameters used are  $\alpha_R = 2$ ,  $\theta = -0.5$ ,  $\kappa = 5000$ ,  $\lambda = 8$ ,  $\gamma = 12$ ,  $\varepsilon = 0.005$ , and  $\beta = 1000$ .

The value  $\alpha_R$  is the coupling strength and the interaction term is a sigmoid that mimics excitatory synaptic coupling. The value of  $\kappa$  modifies the steepness of this sigmoid and we use  $\kappa \gg 1$ . Increasing the value of  $\alpha_R S(x)$  results in a raise of the  $x$ -nullcline,  $\dot{x}_i = 0$ . For small values of  $\varepsilon$ , motion in the  $x$ -direction occurs quickly and an oscillator is said to “jump” between the left and right branches of the cubic. When an oscillator jumps up from the left to the right branch, it crosses the threshold of the interaction term,  $\theta$ , and sends “excitation” to the other oscillator. Thus the interaction is either on or off depending on the positions of the oscillator. When an oscillator receives excitation, its  $x$ -nullcline rises by an amount  $\alpha_R$ . This excited oscillator then exhibits dynamics based on its modified phase space. The three pertinent nullclines for this system are pictured in Figure 67. The pertinent values of the  $x$ -nullclines are the  $y$ -values of their local extrema, which are denoted by the lower left knee (**LLK**) and the lower right knee (**LRK**) for the unexcited  $x$ -nullcline, and the upper left knee (**ULK**) and the upper right knee (**URK**) for the excited nullcline. The values of the extrema for the  $x$ -nullclines given in (A.2) are

$$\mathbf{LLK} = (LLK_x, LLK_y) = (-1, -2)$$

$$\mathbf{LRK} = (LRK_x, LRK_y) = (1, 2)$$

$$\mathbf{ULK} = (LLK_x, LLK_y + \alpha_R)$$

$$\mathbf{URK} = (LLK_x, LLK_y + \alpha_R)$$

A basic description of the behavior of (A.2) now follows. Let the oscillators be denoted by  $O_1$  and  $O_2$ . Let both oscillators begin on the lower left branch (LLB), with  $y_2 > y_1$ . We assume that the time an oscillator spends travelling along LLB is longer than the time an oscillator spends on the upper right branch (URB). Because the motion is counter-clockwise along the limit cycle,  $O_1$  leads  $O_2$ . The leading oscillator,  $O_1$ , will reach  $LLK_y$  first, and jump up to the lower right branch (LRB). Since  $O_1$  has crossed the threshold,  $\theta$ , of the interaction term,  $O_2$  will now receive excitation. There are three main classes of trajectories that arise dependent on the position of  $O_2$  on LLB. If  $O_2$  is below  $LLK_y + \alpha_R$  it will jump up to URB. When  $O_2$  crosses the interaction threshold,  $O_1$  will hop from LRB to URB. This trajectory is shown in Figure 68A and Figure 68B. This leads to a contraction in the time difference between the two oscillators. It can be shown that the time difference between the two oscillators on the left branch is greater than the time difference between the oscillators after they have jumped to the right branch. Therefore, the interaction has caused the time difference between the oscillators to shrink. Somers and Kopell [Somers and Kopell, 1993] refer to this as a compression. This compression occurs twice during each period, once for the jump up and again during the jump down, and leads to a geometric decrease in the time difference between the two oscillators.

If, however,  $O_2$  is above  $LLK_y + \alpha_R$  when  $O_1$  jumps up,  $O_2$  will hop to the upper left branch (ULB). Its motion will continue along ULB until it reaches  $LLK_y + \alpha_R$ , at which time it will jump up to URB. This case is shown in Figure 68C and Figure 68D. It can be shown that this trajectory also results in a decrease in the time difference between the two oscillators.

There is a third class of trajectories that is shown in Figure 68E and Figure 68F. Here,  $O_2$  is above  $LLK_y + \alpha_R$  so that  $O_1$  jumps up and traverses LRB before  $O_2$  reaches ULB.  $O_2$  hops from LLB to ULB and then back to LLB while  $O_1$  traverses LRB. For this class of trajectories the time difference between the oscillators decreases only if the coupling strength is above a critical value. Figure 68F indicates that the oscillators become syn-

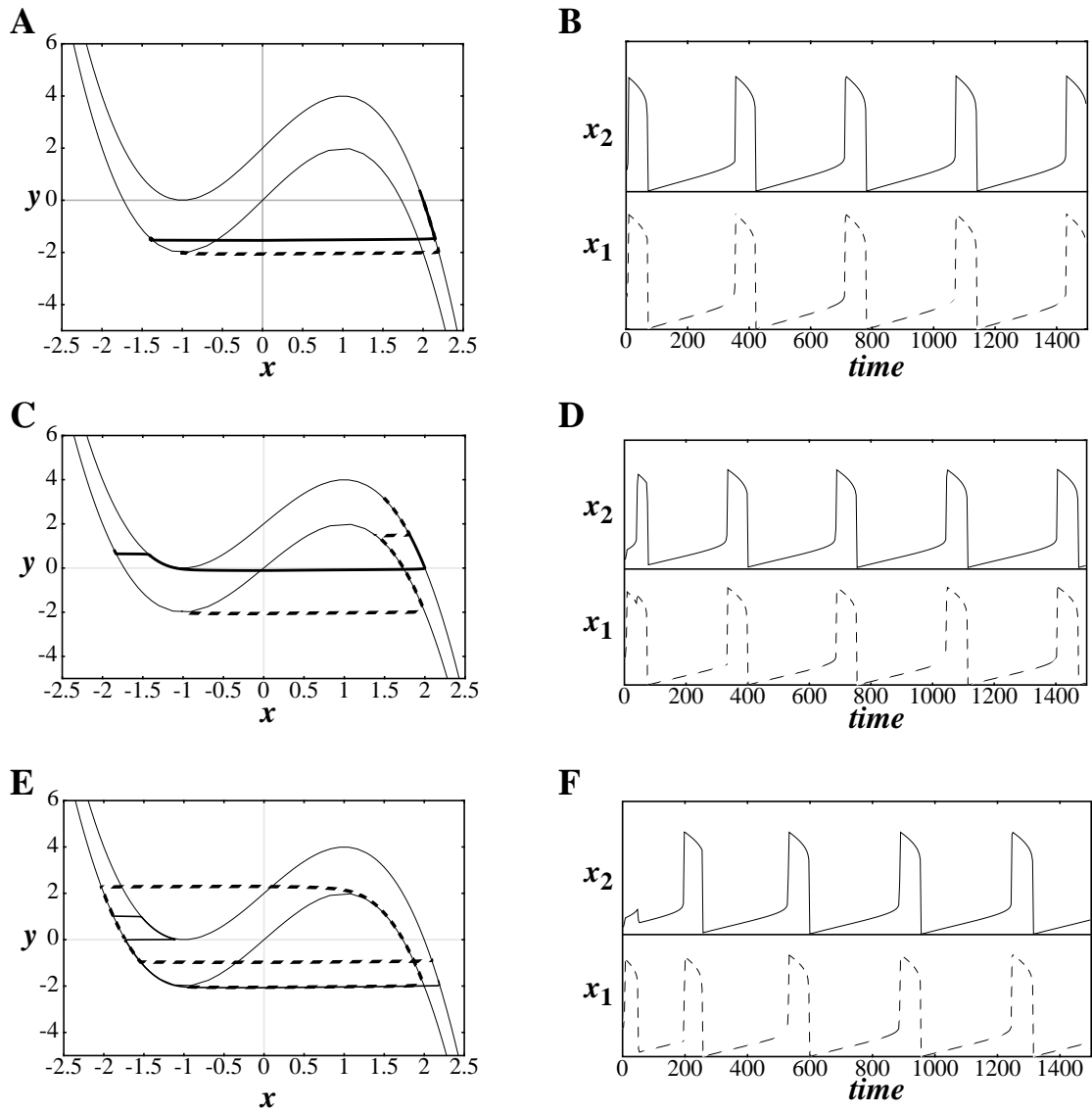


Figure 68. The trajectories of the three cases that lead to synchrony in a pair of coupled oscillators. In (A), (B), and (C) the first oscillator to jump is given by the dotted line and the second is denoted by the solid line. (A), (B) and (C) display the evolution of the system in  $x$ - $y$  space. (D),(E), and (F) display the  $x$ -activities of both oscillators as a function of time. The parameters used are the same as in Figure 67.

chronous. Figure 69A displays a trajectory for initial conditions similar to Figure 68D, but with a coupling strength less than the critical coupling strength. A desynchronous solution results.

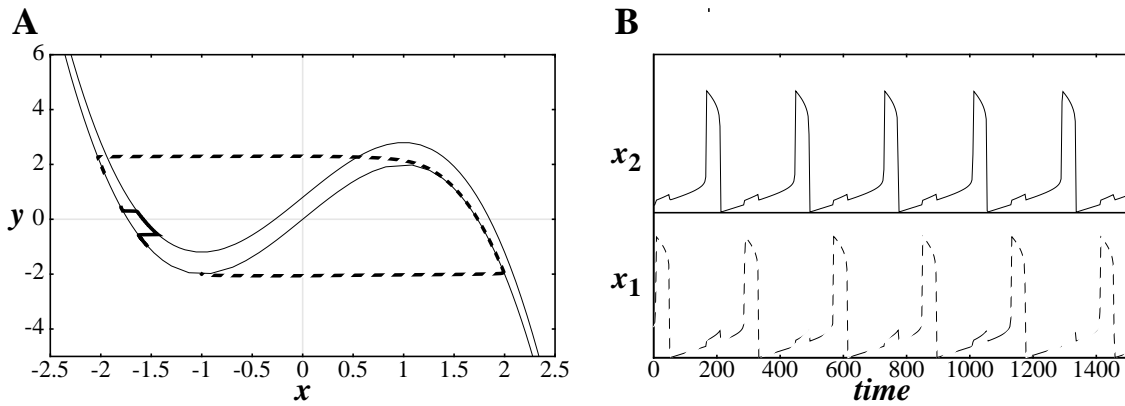


Figure 69. An example of a desynchronous solution that arises because the coupling strength is not large enough. The first oscillator to jump is given by the dotted line and the second is denoted by the solid line. (A) displays the evolution of the system in  $x$ - $y$  space, and (B) displays the  $x$ -activities of both oscillators as a function of time. The coupling strength used was  $\alpha_R = 0.8$  with the other parameters as in Figure 67.